Renewable Energy 139 (2019) 1320–1335

Contents lists available at ScienceDirect

Renewable Energy

journal homepage: www.elsevier.com/locate/renene

Application of the actuator disc theory of Delft3D-FLOW to model far-field hydrodynamic impacts of tidal turbines

V. Ramos [a, *], R. Carballo [b], John V. Ringwood [c]

[a] Interdisciplinary Centre of Marine and Environmental Research of the University of Porto, Terminal de Cruzeiros do Porto de Leixões, Avenida General Norton S/N, 4450-208, Matosinhos, Portugal
[b] Hydraulic Engineering, University of Santiago de Compostela, EPS, Lugo, Spain
[c] Centre for Ocean Energy Research (COER), Maynooth University, Co. Kildare, Ireland

ARTICLE INFO

Article history:
Received 12 April 2018
Received in revised form
5 February 2019
Accepted 16 February 2019
Available online 21 February 2019

Keywords:
Tidal stream energy
HATT
Momentum sink approach
Porous plate
Orkney region

ABSTRACT

Accurate knowledge of tidal turbine impacts on the far-field hydrodynamic conditions, which extend from 3 to 20 diameters downstream the turbine, is essential for the estimation of tidal resource, farm layout design and environmental impact. For this purpose, tidal turbine operation is modelled within coastal models, as enhanced bottom friction, or momentum sinks. In Delft3D-FLOW, a state-of-the-art coastal model, turbine operation is usually represented via momentum losses, using the Porous Plate tool. However, the *Porous Plate* tool presents significant limitations to accurately represent energy extraction and geometry of tidal turbines. Recently, a new tool (*Actuator Disc*) based on the Momentum Actuator Disc Theory (MADT) was developed in Delft3D-FLOW, overcoming the aforementioned limitations and showing excellent results against laboratory data. The aim of this work is to compare the behaviour of the *Actuator Disc* and *Porous Plate* on the far-field hydrodynamics. Overall, significant differences were found, with the *Porous Plate* significantly underestimating the impact on instantaneous and residual flow velocities and turbulence conditions, when the turbine operates at its rated power. Consequently, MADT appears as the best alternative to investigate the far-field hydrodynamic impacts of tidal turbine operation and previous research based on the *Porous Plate* tool should be revisited.
© 2019 Published by Elsevier Ltd.

1. Introduction

In recent years, concerns about the long-term energy supply sustainability, allied with the effects of anthropogenic climate change, have prompted the increased use of renewable energy sources for electricity generation [1]. In this context, tidal stream energy, with an estimated global resource of 1200 *TWh/year* [2], appears as a promising alternative [3], especially given its predictable nature, compared to other renewable sources. Tidal streams are caused by the tidal level variations in conjunction with the morphological characteristics of coastal regions [4]. Consequently, the kinetic energy contained in the tidal currents is harvested by means of Tidal Energy Converters (TECs) placed directly in the flow [5]. Among the variety of TEC concepts, horizontal-axis tidal turbines (HATTs) stand out as the most promising alternative, with several prototypes currently operating under real sea conditions [5].

Tidal turbines operate in complex and harsh coastal systems [6], whose hydrodynamic conditions are determined by a combination of different driving mechanisms such as tides, wave-current interactions, wind and bottom stresses, fresh water discharges and temperature and salinity gradients [7]. In this context, a correct understanding of the interactions between tidal turbines and flow conditions is essential to ensure the viability of tidal farms [8]. On these grounds, according to the distance from tidal turbines, near and far wake disruptions can be distinguished [9].

Near wake spans up to 3 or 4 rotor diameters downstream of the turbine [10]. In this region, the main interest lies in accounting for Blade-Vortex Interaction (BVI) mechanisms [11]. BVI mechanisms govern the highly-unsteady nature of the flow [12], distribution of hydrodynamic loads [13], and boundary layer separation on rotor blades [14], which may considerably impact the efficiency and useful life of tidal turbines. Consequently, to model the aforementioned processes, detailed Computational Fluid Dynamic (CFD) codes, including rotor blade motions and geometry, are required [14].

* Corresponding author.
E-mail address: jvramos@ciimar.up.pt (V. Ramos).

https://doi.org/10.1016/j.renene.2019.02.094
0960-1481/© 2019 Published by Elsevier Ltd.

On the other hand, the flow conditions of the far wake play a crucial role in tidal resource availability [15], tidal farm layout optimisation [16], estuarine circulation [17] and transport of suspended matter (sediments, pollutants and nutrients) [18]. The far wake extends from 3 to 20 rotor diameters downstream the turbine. In this region, the wake starts to widen and flow velocity recovers gradually, as a result of turbulent mixing (with ambient turbulence). The ambient turbulence is therefore more influential than the turbine-generated turbulence, in far wake patterns [12]. As a consequence, the geometry of the rotor blades becomes irrelevant in the determination of the behaviour of the flow, and only the swept area and the thrust force exerted by the turbine during its operation must be considered [19]. As a result, coastal hydrodynamic models, which solve the Reynolds-Averaged Navier-Stokes (RANS) equations under the Boussinesq and shallow-water assumptions, appear as the best tool to model the far wake hydrodynamics of tidal turbines, since the use of detailed CFD codes would be infeasible from a computational standpoint.

Modelling tidal turbine operation within coastal models was traditionally achieved by increasing the bottom drag over small areas representative of either single turbines [16], or tidal farms [20]. Recently, Kramer and Piggott (2016) presented a corrected bottom drag formulation, avoiding grid dependency when computing the thrust force exerted by tidal turbines [21]. Alternatively, tidal turbines can be also modelled by means of local momentum sinks [15]. The main limitations of these methodologies are: (i) inability to account for the turbulence induced by tidal turbine operation via BVI mechanisms, (ii) inaccurate representation of the swept area of the turbine and (iii) assumption of constant values of enhanced drag and momentum loss coefficients, regardless of the Tip Speed Ratio (TSR) of the turbine [22]. Therefore, all these limitations may lead to considerable misrepresentation when addressing relevant issues such as tidal array optimisation and disruptions on the far-field hydrodynamics derived from the operation of tidal turbines.

In this context, the coastal model Delft3D-FLOW [23] has been widely used to assess tidal turbine impact on the far-field hydrodynamics [17], using the *Porous Plate* tool [24]. This tool was originally developed in Delft3D-FLOW to model hydraulic structures as quadratic momentum loss terms [23]. Considering the aforementioned limitations of the momentum sink approach, the *Porous Plate* may lead to significant misrepresentations when modelling the far wake of tidal turbines [22]. Recently, a new feature to model tidal turbines was developed in Delft3D-FLOW [25]. In this case, turbines are modelled as idealised *Actuator Discs*, according to the Momentum Actuator Disc Theory (MADT). MADT was previously applied to model tidal turbine operation within the ocean circulation model ROMS [26], proving its validity to accurately represent the wake effects associated to different configurations of tidal turbine arrays against laboratory test data [27]. Similarly, Mungar proved in Ref. [12], against laboratory test data, that the *Actuator Disc* approach of Delft3D-FLOW, in combination with an adequate model grid size, is capable of modelling the velocity field for the entire far wake with a high degree of accuracy.

Against the foregoing backdrop and, using Delft3D-FLOW as benchmark, this paper aims to evaluate and compare the *Porous Plate* and *Actuator Disc* methodologies to model the impacts of HATT on the far-field hydrodynamics, focusing on hydrodynamic variables such as: (i) free surface elevations, (ii) instantaneous flow velocity (iii) residual flow velocity and (iv) turbulence conditions, whose correct estimation becomes essential for the effective design and viability of tidal farms (e.g. available tidal resource, layout optimisation and environmental impacts). For this purpose, the flow conditions of the Orkney Region, located off the north coast of Great Britain (Fig. 1), were used as a case study.

2. Materials and methods

2.1. Delft3D-FLOW: governing equations

Delft3D-FLOW is a finite-difference hydrodynamic model, which solves a set of equations consisting of momentum, continuity, transport and turbulence closure models [23].

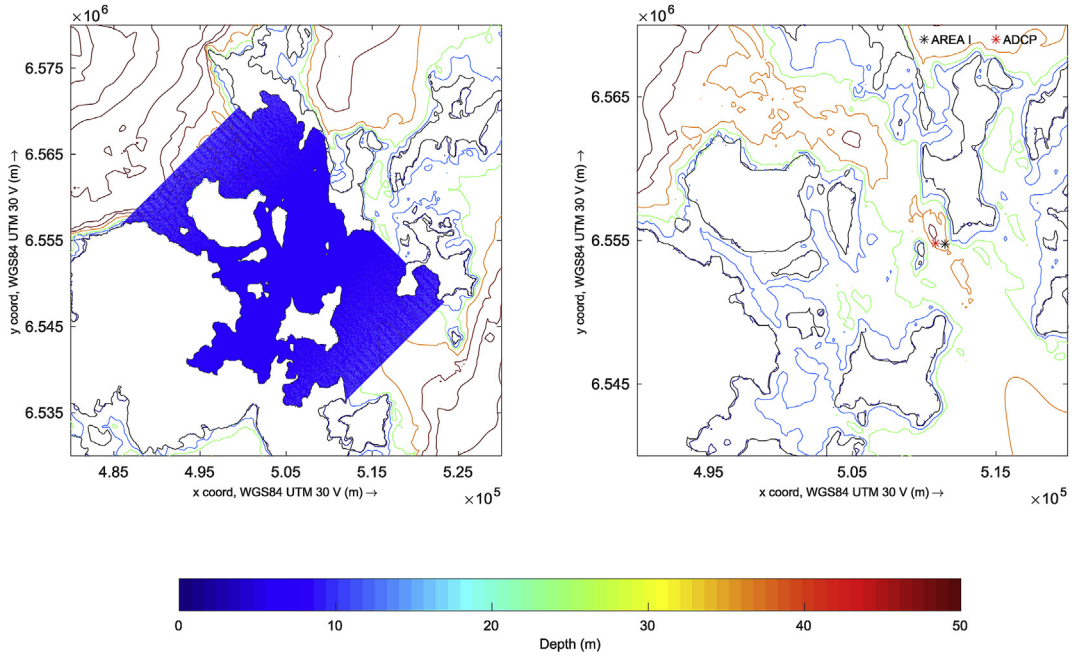

Fig. 1. Orkney region, Scotland (Right). Delft3D-FLOW computational domain (Left side, represented in blue). (For interpretation of the references to colour in this figure legend, the reader is referred to the Web version of this article.)

The conservation of momentum in the vertical direction is simplified to the hydrostatic pressure distribution, p, as a result of the shallow water assumption, in which, accelerations of the flow in the vertical direction, z, can be neglected [28]:

$$\frac{\partial p}{\partial z} = -\rho g, \tag{1}$$

where g is the gravitational acceleration and ρ is the density of sea water, which is computed according to the UNESCO formulation [29].

The momentum equations in the horizontal directions can be expressed as:

$$\frac{Du}{Dt} = +fv - g\frac{\partial \zeta}{\partial x} - \frac{g}{\rho_0}\int_{z'=z}^{z'=\zeta}\frac{\partial \rho}{\partial x}dz' + \nu_H\left(\frac{\partial^2 u}{\partial x^2} + \frac{\partial^2 u}{\partial y^2}\right) + \nu_V\left(\frac{\partial^2 u}{\partial z^2}\right), \tag{2}$$

$$\frac{Dv}{Dt} = -fu - g\frac{\partial \zeta}{\partial y} - \frac{g}{\rho_0}\int_{z'=z}^{z'=\zeta}\frac{\partial \rho}{\partial y}dz' + \nu_H\left(\frac{\partial^2 v}{\partial x^2} + \frac{\partial^2 v}{\partial y^2}\right) + \nu_V\left(\frac{\partial^2 v}{\partial z^2}\right), \tag{3}$$

where ζ stands for the free surface elevation relative to a reference plane ($z = 0$), ρ_o represents the reference density of sea water, f is the Coriolis parameter, u and v are the Eulerian velocity components in the x and y directions, respectively. Finally, ν_V and ν_H stand for the horizontal and vertical eddy viscosity coefficients, and are defined by Eqs. (4) and (5), respectively:

$$\nu_V = \nu_{mol} + max\left(\nu_{3D}, \nu_V^{back}\right), \tag{4}$$

where ν_{mol} is the kinematic viscosity of water, ν_{3D} stands for the fraction of eddy viscosity associated to the 3D turbulence and ν_V^{back} is the background vertical eddy viscosity, which accounts for the vertical turbulent mixing.

$$\nu_H = \nu_{SGS} + \nu_H^{back} + \nu_V, \tag{5}$$

where ν_{SGS} is the sub-grid scale horizontal eddy viscosity, which represents the fraction of the horizontal eddy viscosity associated to turbulent motions and mixing that are not resolved by the horizontal grid. In Delft3D-FLOW, ν_{SGS} is computed by the Horizontal Large Eddy Simulation (HLES) sub-grid model [23]. On the other hand, ν_H^{back} is the background horizontal eddy viscosity, which accounts for the unresolved horizontal turbulent motions. ν_H^{back}, must be defined during the model set-up process and is typically used as a calibration parameter [23].

The mass conservation equation, under the assumption of flow incompressibility, leads to:

$$\frac{\partial u}{\partial x} + \frac{\partial v}{\partial y} + \frac{\partial w}{\partial z} = Q, \tag{6}$$

where w is the vertical component of the Eulerian flow velocity and Q represents the intensity of mass sources per unit area.

The Eulerian velocity vector (u, v, w), can be decomposed into its periodic (u_p, v_p, w_p) and residual components (u_r, v_r, w_r).

$$(u, v, w) = (u_p, v_p, w_p) + (u_r, v_r, w_r), \tag{7}$$

where the residual components (u_r, v_r, v_r) are computed by filtering or time-averaging the Eulerian horizontal velocity components (u, v, w):

$$(u_r, v_r, w_r) = \frac{1}{T}\int_{-T/2}^{T/2}(u, v, w)dt. \tag{8}$$

where T is the cut-off period of the averaging operator.

Flow transport of scalar quantities, such as heat or matter, are modelled by the advection-diffusion equation:

$$\frac{Dc}{Dt} = \frac{\partial}{\partial x}\left(D_H\frac{\partial c}{\partial x}\right) + \frac{\partial}{\partial y}\left(D_H\frac{\partial c}{\partial y}\right) + \frac{\partial}{\partial z}\left(D_V\frac{\partial c}{\partial z}\right) + s \tag{9}$$

with c representing the scalar quantity to be modelled, s is a source or sink term, while D_V and D_H are the vertical and horizontal eddy diffusivity coefficients, which are defined by Eqs. (10) and (11), respectively.

$$D_V = \frac{\nu_{mol}}{\sigma_{mol}} + max\left(D_{3D}, D_V^{back}\right), \tag{10}$$

where σ_{mol} is the Prandtl-Schmidt number for molecular mixing, D_{3D} represents the fraction of eddy diffusivity associated to the 3D turbulence.

$$D_H = D_{SGS} + D_H^{back} + D_V, \tag{11}$$

where D_{SGS} is the sub-grid scale horizontal eddy diffusivity and also is computed by means of the HLES sub-grid model. Finally, D_H^{back} and D_V^{back} are the background vertical and horizontal diffusivity coefficients, which account for other forms of unresolved mixing and, again, are defined during the model implementation.

The flow motion, at turbulent scales, is considered in Delft3D-FLOW by means of the so-called turbulence closure models, which allows computation of the 3D fractions of the vertical eddy viscosity (ν_{3D}) and diffusivity (D_{3D}). Four different turbulence closure models are available in Delft3D-FLOW: constant coefficient, algebraic eddy viscosity model, κ-L model and κ-ε model [23]. For the present work, the κ-ε turbulence closure model was used, since previous works have shown the ability of the κ-ε turbulence model to represent turbulent free-shear flows such as jets or wakes [25,30]. In this context, the transport equation (Eq. (9)) is solved for both the turbulent kinetic energy (κ) and the dissipation rate of turbulent energy (ε). Consequently, the 3D fraction of the vertical eddy viscosity (ν_{3D}) can be obtained by means of Kolmogorov-Prandtl expression:

$$\nu_{3D} = 0.548\sqrt{\kappa}L, \tag{12}$$

where L is the mixing length, given by:

$$L = 0.193\frac{\kappa^{\frac{3}{2}}}{\varepsilon}, \tag{13}$$

On the other hand, the 3D fraction of vertical eddy diffusivity (D_{3D}) is defined as:

$$D_{3D} = \frac{\nu_{3D}}{\sigma_c}, \tag{14}$$

where σ_c is the Prandtl-Schmidt number. Finally, further details regarding the theoretical physics of Delft3D-FLOW can be found in Ref. [23].

2.2. Delft3D-FLOW: tidal turbine modelling

Delft3D-FLOW models the operation of tidal turbines as momentum loss terms [12]. In this context, Delft3D-FLOW presents the so-called *Porous Plate* tool [23], which has been widely used in previous research dealing with turbine modelling in Delft3D-FLOW [15]. A *Porous Plate* is a partially transparent structure with a negligible thickness, covering a certain number of grid layers in the vertical direction. Consequently, the *Porous Plate* generates an additional loss of energy by including two quadratic loss terms (M_x, M_y) on the right-hand side of the momentum equations, Eqs. (2) and (3), which, in this case, account for the momentum removed from the flow due to turbine operation. Therefore, the added momentum terms can be expressed as [23]:

$$M_x = -c_{loss-x}\frac{u^2}{\Delta x}, \tag{15}$$

$$M_y = -c_{loss-y}\frac{v^2}{\Delta y}, \tag{16}$$

where c_{loss-x} and c_{loss-y} are the loss coefficients, which must be set during the implementation of the model. For tidal turbine modelling, c_{loss-x} and c_{loss-y} can be related with the thrust coefficient (C_T) exerted by the turbine according to the methodology defined by Waldman [31]. Therefore, the loss coefficients (c_{loss}), can be defined as:

$$c_{loss-x} = \frac{-2\gamma_x}{\left(1+\sqrt{1-\gamma_x}\right)^2}, \tag{17}$$

$$c_{loss-y} = \frac{-2\gamma_y}{\left(1+\sqrt{1-\gamma_y}\right)^2}, \tag{18}$$

with

$$\gamma_x = \frac{C_T A_{TT} sin\theta}{n\Delta y\Delta z}, \tag{19}$$

$$\gamma_y = \frac{C_T A_{TT} cos\theta}{n\Delta x\Delta z}, \tag{20}$$

where A_{TT} is the total area occupied by the turbine, θ is the angle between the x direction and the turbine axis (Fig. 2), n is the number of vertical layers of the model occupied by the swept area of the rotor and Δx and Δy are the grid discretisation intervals in the x and y directions, respectively.However, this approach was first used to model hydraulic structures [23], with some significant limitations when attempting to extend to tidal turbine operation: (i) the thrust coefficient (C_T) must be assumed constant regardless the incoming flow velocity of the turbine, which may lead to misrepresentation on the momentum-loss terms (Eq. (15) and (16)), (ii) neither *cut-in* nor *cut-out* velocity considerations can be implemented and, therefore, there will be always a removal of momentum from the flow, even when the turbine is not in its range of operation, and (iii) tidal turbines are modelled with misrepresentations regarding the swept area of the rotor, since the *Porous Plate* must cover the complete vertical surface of one or more grid cells (Fig. 4). In spite of all these limitations, this methodology appeared to be the most viable alternative to investigate the far-field (of the order of several rotor diameters away from the turbine) impacts of tidal energy extraction, since the size of the area of study would make the use of CFD codes computationally infeasible [16].Recently, a new feature was developed in Delft3D-FLOW to address the limitations of the *Porous plate* approach [25], using Momentum Actuator Disc Theory (MADT). In this case, the turbines are modelled as idealised *Actuator Discs*, with negligible thickness, in the normal direction of the flow. Again, the sink terms expressed in Eqs. (15) and (16) are used to account for the momentum removed from the flow. The loss coefficients (c_{loss}), can be derived from the thrust coefficient (C_T):

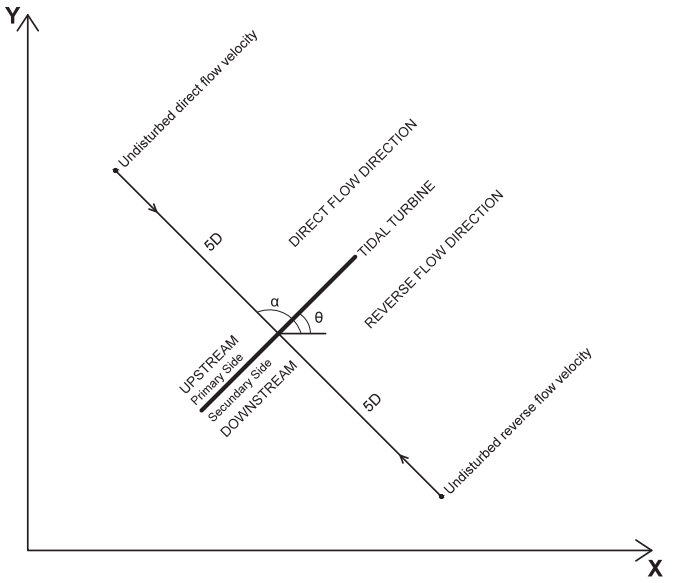

Fig. 2. Schematic representation of tidal turbines in Delft3D-FLOW.

$$c_{loss-x} = \frac{1}{2}C_T\frac{u_0^2}{u^2}, \tag{21}$$

$$c_{loss-y} = \frac{1}{2}C_T\frac{v_0^2}{v^2}, \tag{22}$$

where u_0 and v_0 represent the components of undisturbed flow velocity. Therefore, this definition avoids operational misrepresentation caused by the disturbed flow velocity in the vicinity of the turbines. Delft3D-FLOW assumes that the values of the undisturbed flow velocity (u_0, v_0) are coincident with the flow velocity at positions located a certain number of rotor diameters upstream/downstream normal to the turbine's rotor (Fig. 2). Additionally, the thrust coefficient can be defined as a function of the flow velocity, assuming a constant value across the surface of the *Actuator Disc*. Only horizontal axis with a circular rotor shape can be considered, in which the position and swept area of the rotor is represented in the vertical domain as represented in Fig. 4. The swept area of the rotor turbine is represented by the vertical grid cells lying inside the rotor surface. For the grid cells in which the turbine is partially present (i.e. outer limits of the rotor surface), the area of those elements is given by the sum or subtraction of circle segments, triangles and rectangles [23]. With respect to the vertical position of the turbines, two configurations are available: (i) bottom-fixed, whose frame is assumed to not be sensitive to bed level changes or (ii) floating, with the frame responding to water level variations. In contrast to Roc et al. [26], this methodology does not consider the turbulence effects caused by Blade-Vortex Interaction (BVI) mechanisms, which may play a significant role in problems dealing with tidal farm layout optimisation [27]. Consequently, for future developments, the turbulence closure models available in Delft3D-

Table 1
Main technical characteristics of the horizontal-axis tidal turbine proposed by Baston et al. (2015).

Type	Seabed fixed
Foundation	Monopile
Diameter (m)	20
Cut-in velocity (ms^{-1})	1.0
Cut-off velocity (ms^{-1})	4.0
Rated velocity (ms^{-1})	2.5
Rated power (MW)	1–1.5

FLOW must include new terms to account for BVI mechanisms such as blade root and tip vortices and wake rotational motions and vortices [26].

Mungar investigated in Ref. [12] the validity of the *Actuator Disc* methodology against laboratory test data for horizontal-axis tidal turbines (HATTs) [32], proving that Delft3D-FLOW is capable of predicting both the shape of the individual, and merged wakes, induced during HATT operation. From 5 rotor diameters downstream of HATTs, Delft3D-FLOW is able to compute the velocity field with discrepancies in terms of normalized velocity deficit and stream wise turbulence intensity lower than 15 %. Moreover, Mungar also found that the accuracy of the model is highly sensitive to grid resolution. Therefore, when the horizontal grid size is larger than the rotor diameter, Delft3D-FLOW struggles to model the near wake (up to 5 rotor diameters downstream of the HATTs), producing accurate results from approximately 7 rotor diameters downstream of HATTs. For the vertical distribution of the grid, negligible differences between σ-layer and *Z*-layer models were found and, again, vertical grid sizes smaller than the rotor diameter offer better results. In summary, Delft3D-FLOW appears to be a promising tool to accurately estimate the far-field impact of tidal energy extraction, at reasonable computational cost.

2.3. Delft3D-FLOW: model implementation

A 3D hydrodynamic model was implemented for the area of study (Fig. 1), following the recommendations proposed by the International Electrotechnical Commission (IEC-62600-201) for tidal stream resource characterisation [6]. For the vertical discretisation of the model, a distribution of eight σ-layers is prescribed, using a variable thickness alongside the water column (Fig. 4). Therefore, areas close to the water surface and seabed present higher resolution than the middle layers (2.5-5-7.5-15-22.5-22.5-15-7.5-5-2.5% of the local water depth) to address, in detail, the relevant physical processes that take place at those layers (bottom and wind stresses). On the other hand, for the horizontal discretisation, a Cartesian grid was used, with a variable resolution, increasing from a minimum grid size of $20 \times 20\ m$ towards the open boundaries (Fig. 1). Following [15], the minimum grid size was chosen to match the diameter of the rotor of the HATT used for the present study (Table 1). The bathymetric data for the region was obtained from the General Bathymetric Chart of the Oceans (GEBCO) datasets, which were interpolated onto the computational domain of the model by means of the Delft3D-QUICKIN toolbox.

For the model set-up, boundary free surface elevations and Coriolis forcing were considered. Previous studies of the region [33], have shown that density gradients were too low to present a significant effect on the hydrodynamic behaviour of the region. Furthermore, no significant river discharges were found at the area of study and, therefore, no additional flow sources were included in the model. The boundary conditions consisted of time-series (10 min interval) of the free surface elevations, which were obtained from a large-scale regional model, by means of a nesting approach. Further details regarding the main characteristics of the regional model can be found in Ref. [34]. With respect to the κ-ε turbulence closure model used for the present work, the terms (ν_{SGS}, D_{SGS}) computed by the HLES sub-grid model were not considered, since their effect when predicting the wakes generated by the HATTs can be considered negligible [25]. In addition, the background horizontal eddy viscosity (ν_H^{back}) and diffusivity (D_H^{back}) coefficients were set to 30 $m^2 s^{-1}$ after a calibration procedure. For the bottom roughness, the Manning coefficient was defined as a function of the water depth, following Dias and Lopes [35]. Finally, at the land margins the boundary conditions were null velocity and free slip (zero shear stress).

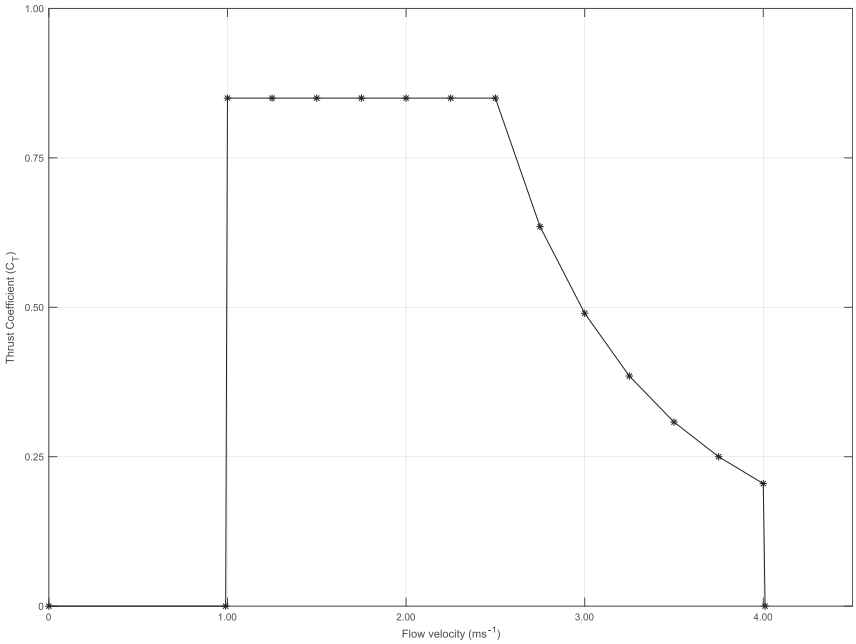

Fig. 3. Thrust coefficient curve of the horizontal-axis tidal turbine proposed by Baston et al. (2015).

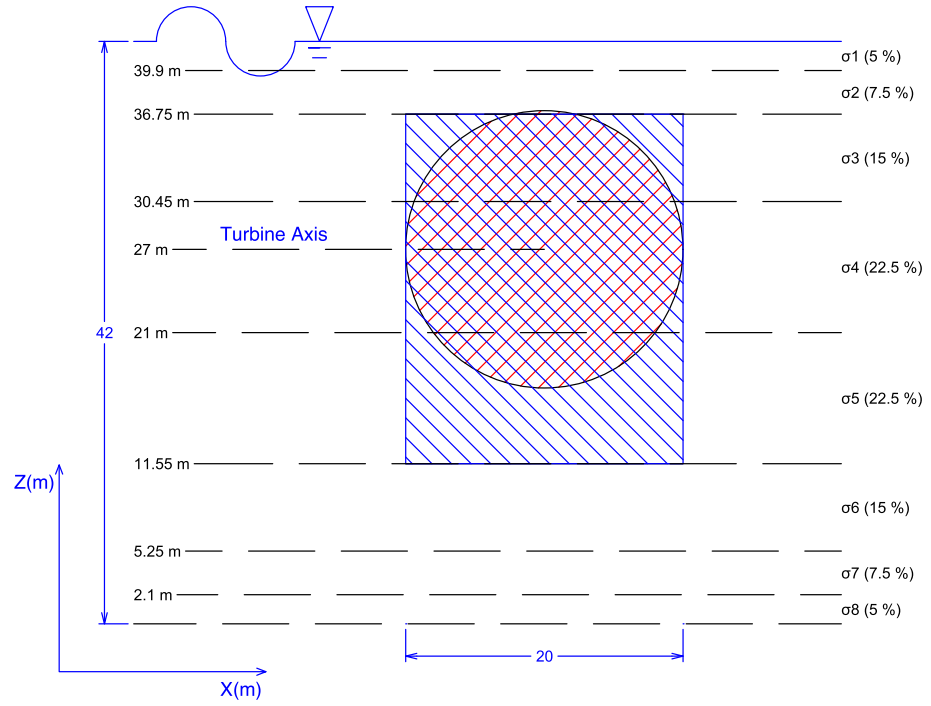

Fig. 4. Schematic representation of the *Actuator Disc* (Red Shading) and *Porous Plate* (Blue Shading) in Area I. (For interpretation of the references to colour in this figure legend, the reader is referred to the Web version of this article.)

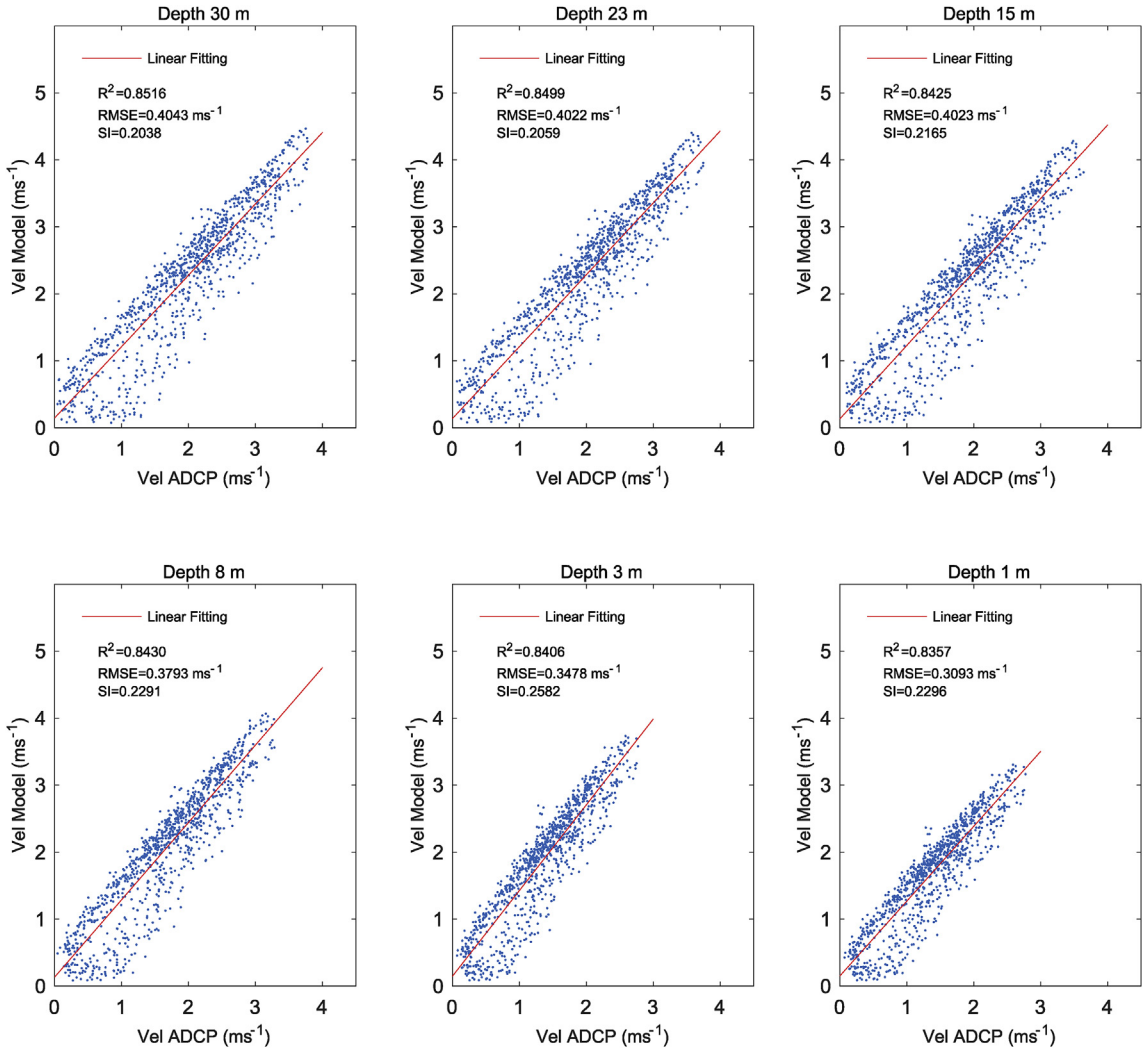

Fig. 5. Delft3D-FLOW model validation.

2.4. Delft3D-FLOW: model validation

The hydrodynamic model was validated against recorded flow data obtained from an ADCP located at the EMEC Fall of Warness tidal site (59°07.940′ N, 2°48.688′ W, WGS84), where the mean recorded depth was 40.8 *m*. ADCP measurements covered a period of 38 days from 3rd April to 11th May 2009. The validation simulation was implemented using the so-called *hot-start* approach. The initial conditions were obtained from a previous simulation, in which the model was spun up during a two week-period with the purpose of adjusting the flow field and, therefore, do not affect the numerical results during the validation period. Finally, the validation was carried out at six different water depths, in order to ensure that the flow is accurately computed across the water column.

Fig. 5 shows the linear regression fitting for the absolute flow velocity, for all the considered water depths, along with the corresponding statistical analysis (Determination Coefficient, R^2, Root Mean Square Error, *RMSE*, and Scatter Index, *SI*). In general, good agreement was found at all water depths, with values of R^2 and *RMSE* of the order of 0.85 and 0.35 ms^{-1}. The main differences were found at the peak velocities, especially at the deepest layers where the model seems to slightly underestimate the peak tidal flows.

2.5. Hydrodynamic far-field impacts: study cases

Upon validation, the model was applied to compare the impact that would result from the operation of tidal turbines according to the two procedures available in Delft3D-FLOW: *Porous Plate* and *Actuator Disc* (Section 2.2). The generic horizontal-axis tidal turbine (HATT) proposed by Baston et al. in Ref. [22], was used for the present study, whose main technical characteristics are presented in Table 1. Additionally, Fig. 3 shows the variation in the thrust coefficient (C_T) in terms of the undisturbed flow velocity at the rotor axis.

For this purpose, real flow conditions were used (Orkney Region, Fig. 1). Therefore, local effects on the operating flow conditions of HATTs, such as rapid bathymetric changes, wind, and tidal asymmetries were accounted for. Three different simulations were run for a period corresponding to a complete tidal cycle (i.e. 24 h 50 m). Two simulations were implemented, considering the operation of a single HATT placed in Area I (Fig. 1), which correspond to the *Porous Plate* and *Actuator Disc* cases. For the *Porous Plate* case, the loss coefficient terms (c_{loss}) were obtained using equations (17) and (18), considering a representative and constant value of the thrust coefficient (C_T) of 0.7 (Fig. 3), whereas the rotor swept area is roughly approximated to the vertical surface of the grid cells covering from σ-layer 3 to 5 (Fig. 4). Conversely, for the *Actuator Disc* case, the loss coefficient terms were computed by means of equations (21) and (22) considering the dependence of the thrust coefficient with the flow velocity (Fig. 3), while the rotor surface was accurately represented using the rotor diameter and nacelle's water depth (Table 1) as model inputs. In addition, a simulation without considering tidal energy extraction was run to compare the effects of HATT operation with the undisturbed flow conditions (*Undisturbed* case).

In this context, the far-field impacts derived from HATT energy

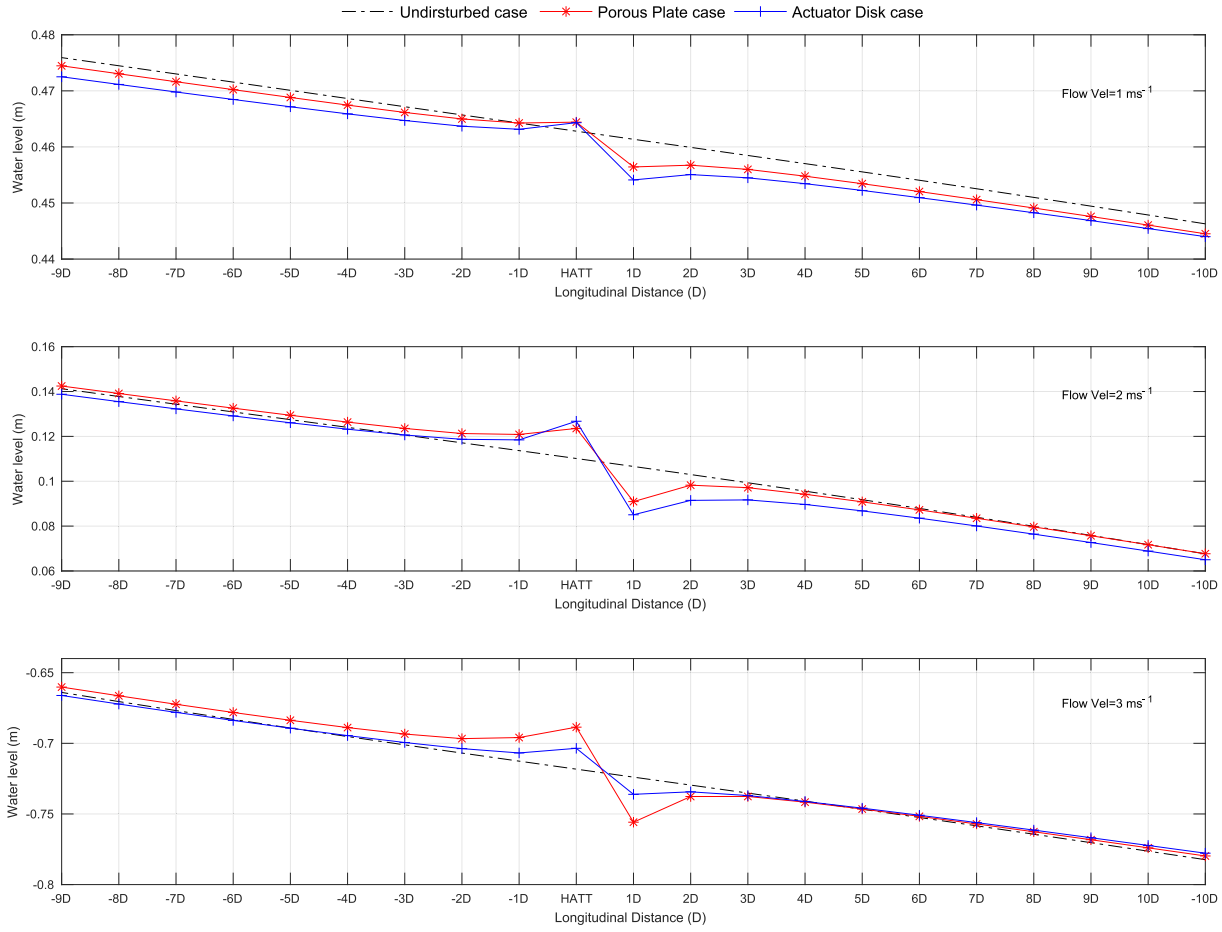

Fig. 6. Comparison between the Porous Plate and Actuator Disc approaches: Impacts on the longitudinal profiles of the free surface elevation.

extraction were investigated for relevant hydrodynamic variables such as: free surface elevations (Section 3.1), instantaneous flow velocity (Section 3.2), residual flow velocity (Section 3.3) and turbulence conditions (Section 3.4). For instance, disruption of the instantaneous flow velocity may alter the available tidal resource [15] and the optimal layout of the tidal farm [36]. Residual flow velocities correspond to the instantaneous flow velocities averaged over a period of time, usually a tidal cycle (Eq. (9)). The magnitude of the residual velocities is of the order of ζ/H, where ζ is the free surface elevation and H the local water depth, and they are strongly influenced by local effects of wind, salinity gradient, river discharges and tidal asymmetry [37]. Therefore, non-zero values of residual flow velocity, is equivalent in practical terms to a "*permanent*" current in the estuary, which will be the main driving force of mass transport (sediments, nutrients, pollutants) [18]. Lastly, high-energy turbulent conditions, characteristic of tidal energy sites [38], play a crucial role in terms of structural and fatigue loads on the turbine blades [39], generated wakes [40], and power extraction [41]. Consequently, correct estimation of all those variables is essential to predict the techno-economic feasibility and potential environmental impacts of a tidal farm.

3. Results

3.1. Far-field impacts: water levels

Fig. 6 shows the longitudinal variation (section normal to the HATT rotor) of the free surface elevation. Overall, as the incoming flow approaches the turbine, the water level increases, reaching its maximum value at the rotor surface. Downstream of the HATT, the free surface elevation experiences a significant drop associated with the momentum extraction of the turbine. From that point on, the water level tends to recover its unaltered value as the flow moves further away from the HATT. However, the global alterations in the free surface elevation can be considered negligible, with maximum variations up to 0.07 m (Flow velocity of 3 ms^{-1}). Fig. 7 shows the lateral variation of the free surface elevation downstream of the HATT (sections parallel to the HATT rotor). The results obtained show that the lateral water level variation is almost negligible 3 rotor diameters downstream of the HATT.

Comparing the response for the *Porous Plate* and *Actuator Disc*, minor differences are found, with both approaches showing similar trends. However, for high values of flow velocity (3 ms^{-1}), the *Porous Plate* overestimates water level variations (lateral and

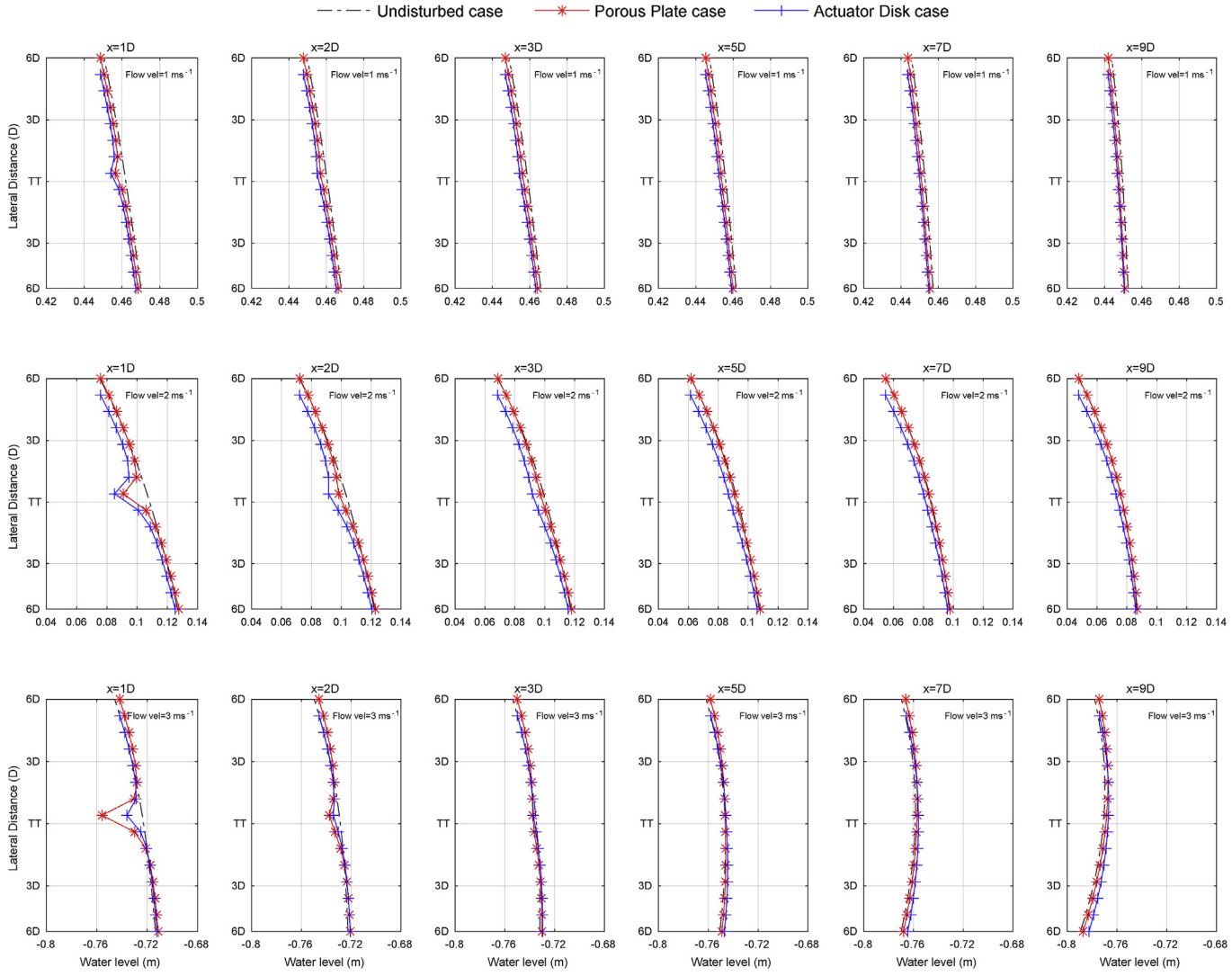

Fig. 7. Comparison between the Porous Plate and Actuator Disc approaches: Downstream impacts on the lateral profiles of the free surface elevation.

longitudinal) in the vicinity of the HATT. In this case, the *Porous Plate* is computing the coefficient loss terms (c_{loss}) assuming a constant value of the thrust coefficient (C_T=0.7), while according to Fig. 3, C_T takes a value of around 0.5. In addition, the quadratic dependence of the momentum loss terms (M_x and M_y) on the flow velocity, amplifies the errors related to the C_T assumptions.

3.2. Far-field impacts: instantaneous flow velocity

The longitudinal disruptions of the flow velocity, at the water depth corresponding with the hub of the HATT, are shown in Fig. 8. Overall, the flow velocity experiences drops (up to 0.3 ms^{-1}) when encountering the rotor turbine, which become more evident as the tidal flow velocity increases. This behaviour results from the quadratic nature of the momentum loss terms computed by the *Porous Plate* and *Actuator Disc* approaches (Eqs. (14) and (15)). Downstream, the velocity tends to increase again, but only for the case of a tidal flow of 1 ms^{-1} is it able to recover its undisturbed value (6 rotor diameters downstream of the HATT). Conversely, for tidal flows of 2 and 3 ms^{-1}, the amount of momentum removed from the flow is significantly greater (Eqs. (14) and (15)) and, therefore, the flow struggles to recover its undisturbed profile. The recovery of the wake downstream of the HATT is governed by turbulent mixing, in which the ambient flow transfers energy to the flow within the wake.

Fig. 9 shows the evolution of the wakes induced by the HATT. It can be observed that the wake flattens and increases its width as the downstream distance from the HATT increases. Nonetheless, only for tidal flows of 1 ms^{-1}, ambient turbulence is capable of recovering the undisturbed shape of the wake (9 rotor diameters downstream of the HATT). Finally, the variations in the vertical velocity profile are highlighted in Fig. 10. The presence of the turbine diverts part of the flow, which is accelerated through narrower sections. In contrast, the flow facing the rotor loses momentum, resulting in a velocity reduction. As the flow moves further away from the HATT, the vertical profile tends to recover its logarithmic shape.

In general, considerable differences were found when comparing the results obtained with the *Porous Plate* and *Actuator Disc* approaches. In terms of the longitudinal and vertical profiles, the *Porous Plate* approach seems to misrepresent the velocity drop at the HATT and the recovery profile downstream of the HATT (Figs. 8 and 10). Regarding the prediction of the wake generated by the HATT (Fig. 9), both approaches show similar results in terms of the wake width. However, considerable differences regarding flow decelerations (facing the rotor) and accelerations (bypassing the rotor) were found. This behaviour can be explained via the limitations of the *Porous Plate* approach. Firstly, a rectangular rotor geometry must be adopted (spanning the vertical surface of grid cells corresponding to σ-layers 3, 4 and 5), whereas, for the *Actuator Disc*, the position and shape of the rotor can be defined according to the true geometric characteristics of the HATT (Fig. 4). Secondly, a constant loss coefficient must be associated with a representative value of the HATT thrust coefficient (C_T). For the present study, C_T is set to an average operating value of 0.7 (Section 2.2). However, when the HATT operates with incoming flows of 1 and 2 ms^{-1}, the

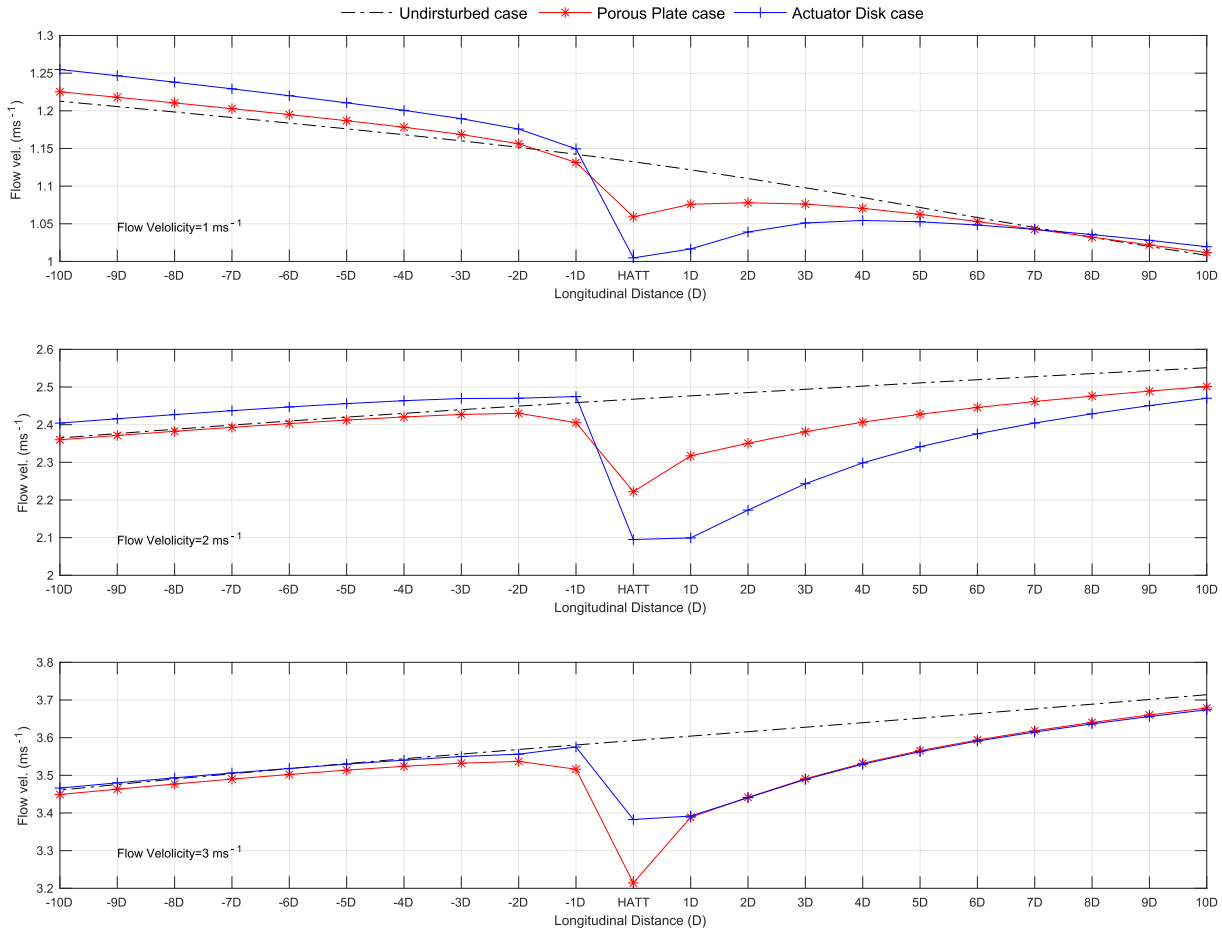

Fig. 8. Comparison between the Porous Plate and Actuator Disc approaches: Impacts on the longitudinal profiles of the instantaneous flow velocity at the HATT's hub water depth.

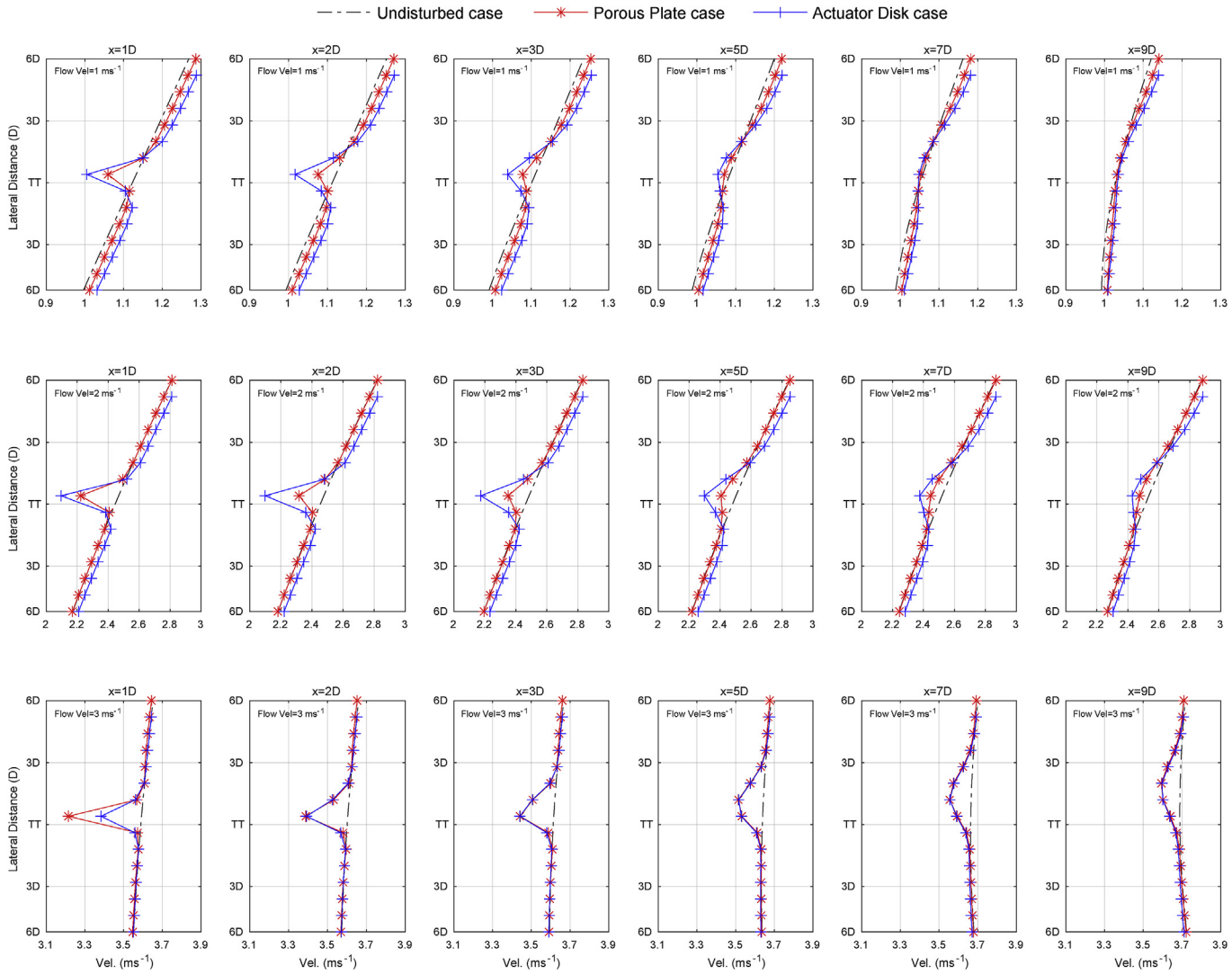

Fig. 9. Comparison between the Porous Plate and Actuator Disc approaches: Downstream impacts on the lateral profiles of the instantaneous flow velocity at the HATT's hub water depth.

actual value of C_T is 0.85 while, for the case of 3 ms^{-1}, C_T drops to 0.5 (Fig. 3). Taking into account these two facts, the *Porous Plate* methodology misrepresents both the swept area and the amount of momentum extracted during HATT operation, which are the main differences between the *Porous Plate* and *Actuator Disc* approaches, in terms of blockage effects and bypass acceleration of the flow.

3.3. Far-field impacts: residual flow velocity

The components of the residual flow velocity were determined according to Eq. (9). Orkney tides are strongly semi-diurnal [42]; therefore, the averaging period (T) is set to a value corresponding with the period of the principal semi-diurnal lunar (M2) constituent ($T = 12.42$ h), covering the complete variability of the tide [43].

Overall, a strong residual flow was found in Area I, with values up to 0.3 ms^{-1}. This residual flow can be explained by the pronounced tidal asymmetry present in the region [42]. Furthermore, residual flow profiles (Fig. 11) show a similar behaviour to those observed in the instantaneous flow velocity (Figs. 8–10). However, the relative differences, with respect to the unaltered conditions, are considerably higher. Longitudinal and vertical profiles show remarkable differences, both upstream and downstream of the HATT, with the *Porous Plate* underestimating the residual velocity drop at the HATT hub by approximately 30% compared to the *Actuator Disc*. Additionally, convergence on the residual profiles is only reached after 7 rotor diameters downstream of the HATT. Again, those differences are associated with the limitations of the *Porous Plate*, which are explained in detail in Section 3.2.

Finally, and considering that the residual flow acts as the main driving force of suspended mass transport, significant divergence can be expected when modelling the impacts associated with HATT operation on relevant variables such as sediment, nutrient and pollutant transport.

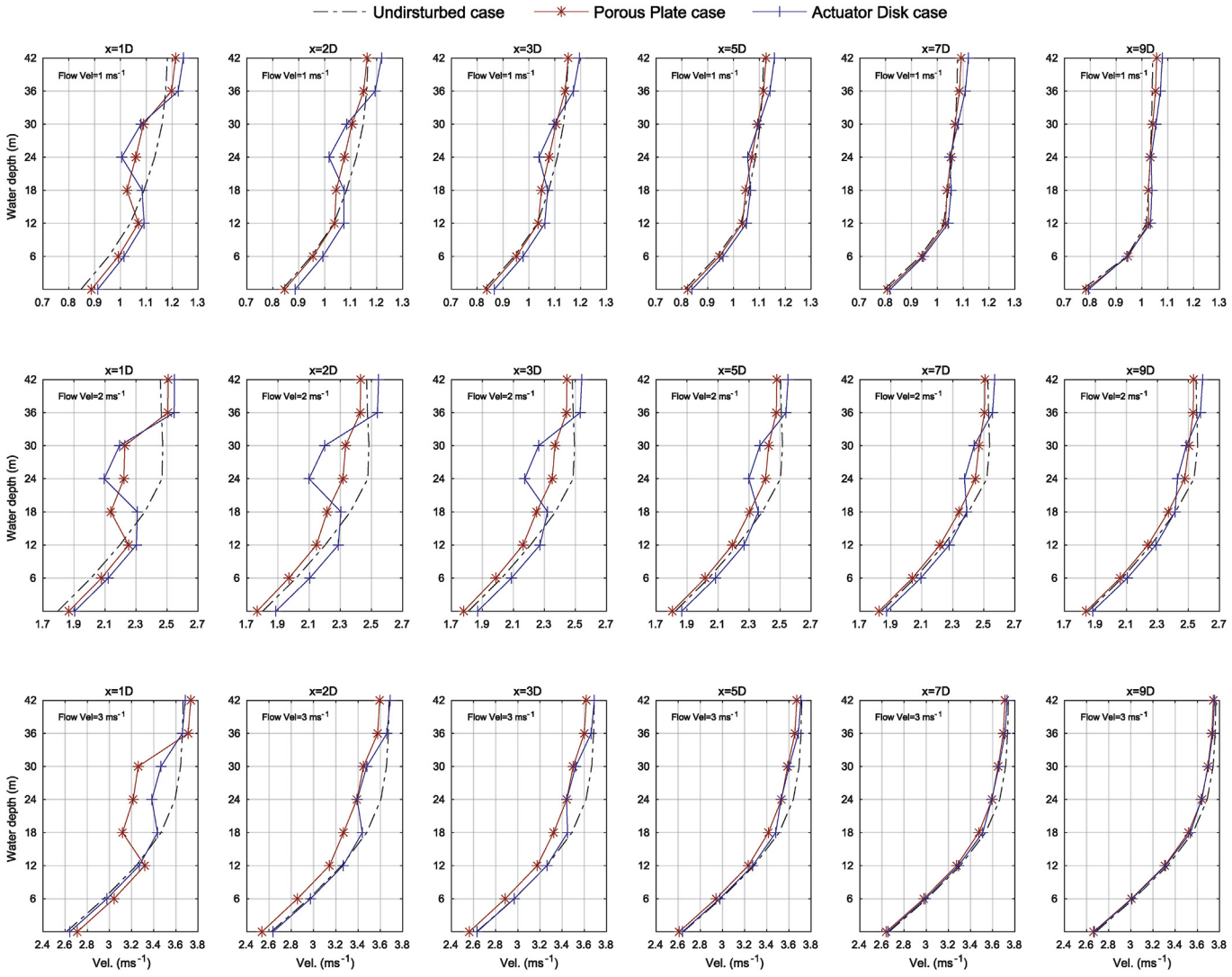

Fig. 10. Comparison between the Porous Plate and Actuator Disc approaches: Downstream impacts on the vertical profiles of the instantaneous flow velocity.

3.4. Far-field impacts: turbulent kinetic energy

The effects of HATT operation on the turbulence conditions were assessed in terms of Turbulent Kinetic Energy (TKE), which represents the energy stored in turbulent fluctuations per kilogram of fluid [38].

The disruption on the TKE, in terms of the longitudinal, lateral and vertical profiles, is shown in Figs. 12–14, respectively. The turbulence induced by HATT operation translates into significant increases of TKE values, which are especially noticeable for its longitudinal and vertical profiles. In this context, when the HATT operates at its rated power (1–2.5 ms^{-1}, Fig. 3), TKE reaches values four times higher than the undisturbed flow conditions, as can be observed in Figs. 12 and 14. Finally, as the flow moves further away from the HATT, the TKE profiles tend to recover their undisturbed values due to turbulent mixing, but the disruptions are still noticeable after 10 rotor diameters.

As mentioned in previous sections, significant differences between the *Porous Plate* and *Actuator Disc* were found. In this case, HATT geometry assumptions (*Porous Plate*) do not appear to play an important role, as shown in Fig. 13, where the differences in the wake width are largely irrelevant. However, the assumption of a constant thrust coefficient (C_T=0.7) for the *Porous Plate* case, introduces significant errors (see Section 3.2), with underestimations of TKE (close to 30 %) within the HATT's rated velocity range (1–2.5 ms^{-1}). Conversely, for high velocity flows (3 ms^{-1}) the *Porous Plate* approach overestimates the TKE variations up to 20%.

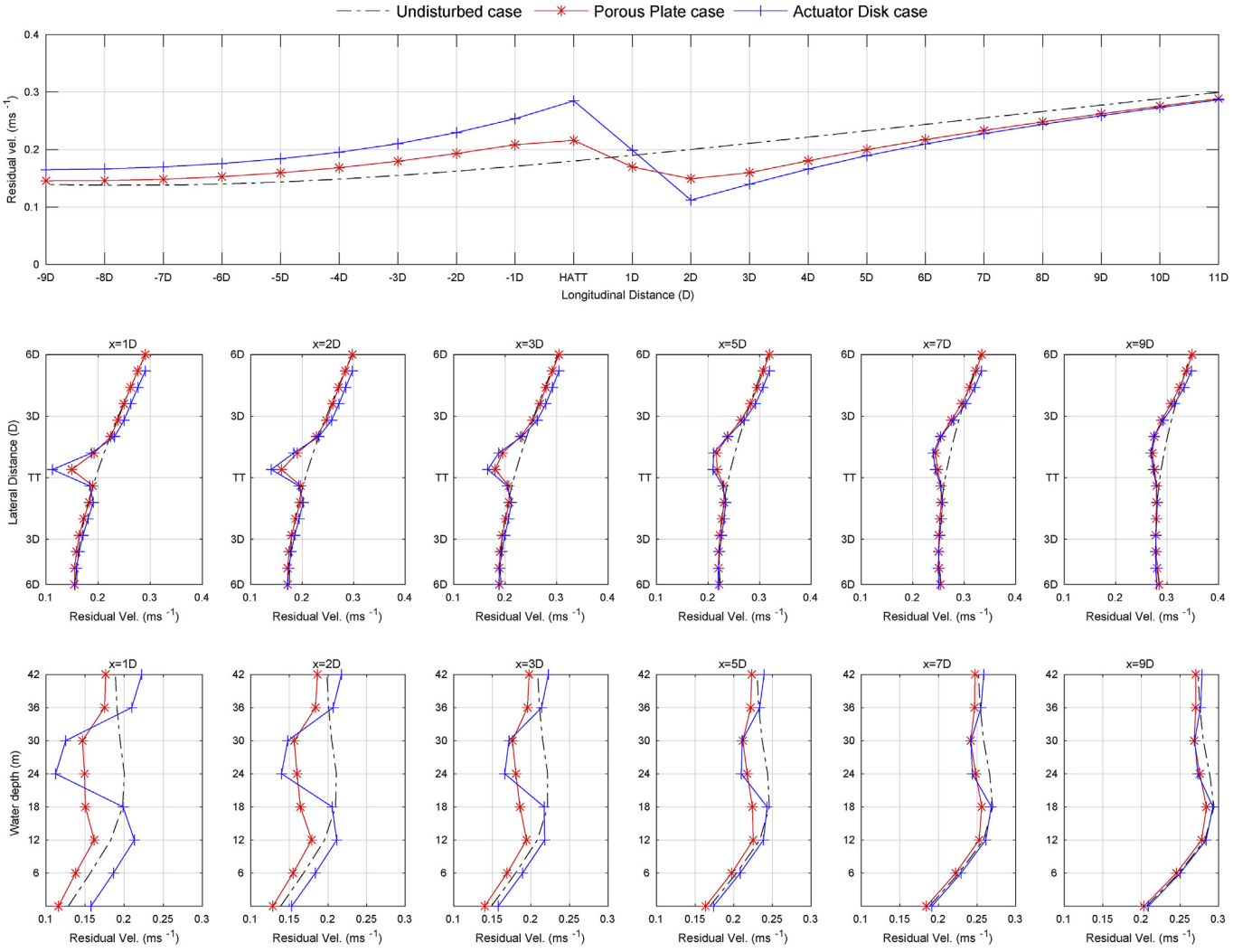

Fig. 11. Comparison between the Porous Plate and Actuator Disc approaches: Impacts on the longitudinal (Upper), lateral (Middle) and vertical (Bottom) residual flow velocity.

4. Discussion

This section presents a discussion about the two main topics tackled in this investigation: (i) the characteristics of the methodologies available in Delft3D-FLOW to model tidal turbine operation (*Porous Plate* and *Actuator Disc* approaches) and (ii) the differences between each methodology in estimating the impact on far-field hydrodynamics.

Both approaches, *Porous Plate* and *Actuator Disc*, model tidal turbine operation as momentum sink terms, which are related to the thrust exerted by the turbine during its operation. However, significant differences can be found. Firstly, the *Porous Plate* approach models turbine operation assuming constant loss coefficient terms based on representative values of the thrust coefficient (e.g. $C_T = 0.7$), whereas the *Actuator Disc* defines variable loss coefficient terms, associated with the variation of the thrust coefficient during turbine operation (Fig. 3). In this context, as the incoming tidal flow velocity increases, the differences in the momentum loss terms computed by both approaches becomes more evident, according to the quadratic dependency with the flow velocity of Eqs. (15) and (16). Secondly, for the representation of the swept area of the turbine, the *Porous Plate* assumes that the rotor covers the complete surface of a certain number of vertical gird cells, always resulting in a rectangular shape and grid-size related. In contrast, for the *Actuator Disc*, the rotor swept area is defined based on the diameter of the blades and the water depth of the nacelle's turbine.

On these grounds, the results obtained confirm that the *Porous Plate* and *Actuator Disc* approaches show considerable differences when modelling the effects on the far-field hydrodynamics

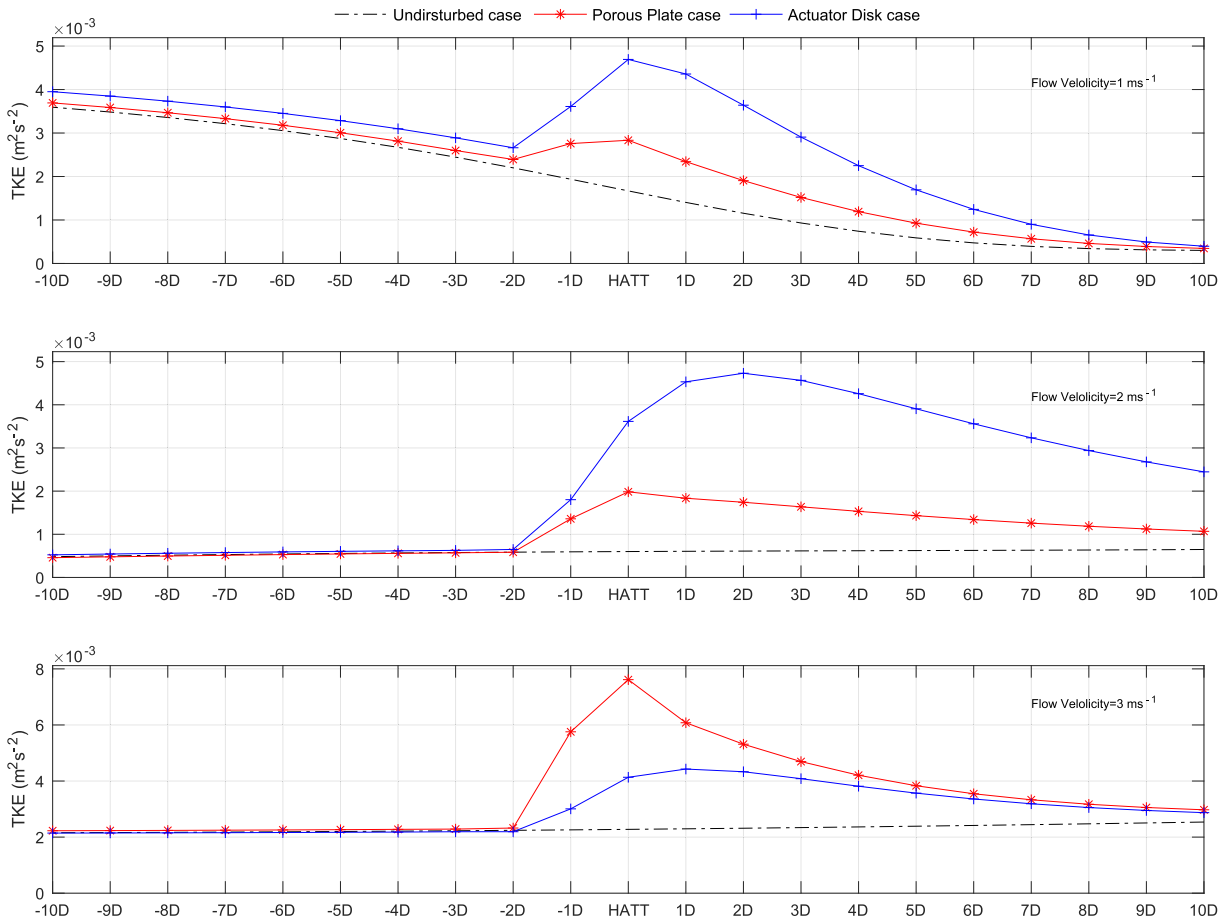

Fig. 12. Comparison between the Porous Plate and Actuator Disc approaches: Impacts on the longitudinal profiles of the instantaneous TKE at the HATT's hub water depth.

associated with tidal turbine operation. When the HATT is operating in its rated range (from 1 to 2.5 ms^{-1}, Fig. 3), the *Porous Plate* approach seems to underestimate the disruptions created in the near and far wakes. For example, the relative difference in TKE profiles reaches values of up to 30% (Fig. 12), while for the instantaneous and residual velocity profiles, lower but still significant differences were found (up to 10%). Conversely, for tidal flow velocities higher than 2.5 ms^{-1}, the tendency is reversed, with the *Porous Plate* overestimating the impacts caused on the near wake (up to 3 rotor diameters downstream). This fact highlights that the representation of the loss coefficient terms (constant for the *Porous Plate* vs. velocity dependent for the *Actuator Disc*) and the consideration of the cut-in and cut-out turbine velocities (*Actuator Disc*) are of greater importance than the geometric representation of the rotor's turbine. Finally, it is worth mentioning that significant divergences related to the rotor surface were not expected, since the horizontal resolution of the computational grid was matched to the diameter of the HATT (20 m). However, as the grid size increases, with respect to the rotor's diameter, considerably higher differences on the far-field hydrodynamics are expected, which emphasises the high dependence of the *Porous Plate* on the grid resolution, as can be observed in Fig. 4.

5. Conclusions

In order for tidal stream energy to become a commercially viable energy source, accurate understanding of the far-field hydrodynamic impacts derived from tidal turbine operation is required. For instance, variations in the instantaneous flow velocity may alter the available tidal resource and the optimal farm layout, estimated according to the undisturbed flow conditions. Furthermore, disruptions of residual flows could modify the natural transport patterns of suspended matter (e.g. sediments, nutrients and pollutants). Finally, modifications in terms of turbulence conditions may result in remarkable impacts on power extraction, wake generation and fatigue loads of tidal turbines.

In this context, the traditional approach to determine far-field impacts of tidal energy extraction consists of modelling turbine operation within coastal models (e.g. Delft3D-FLOW). For this purpose, methodologies which represent tidal turbines as

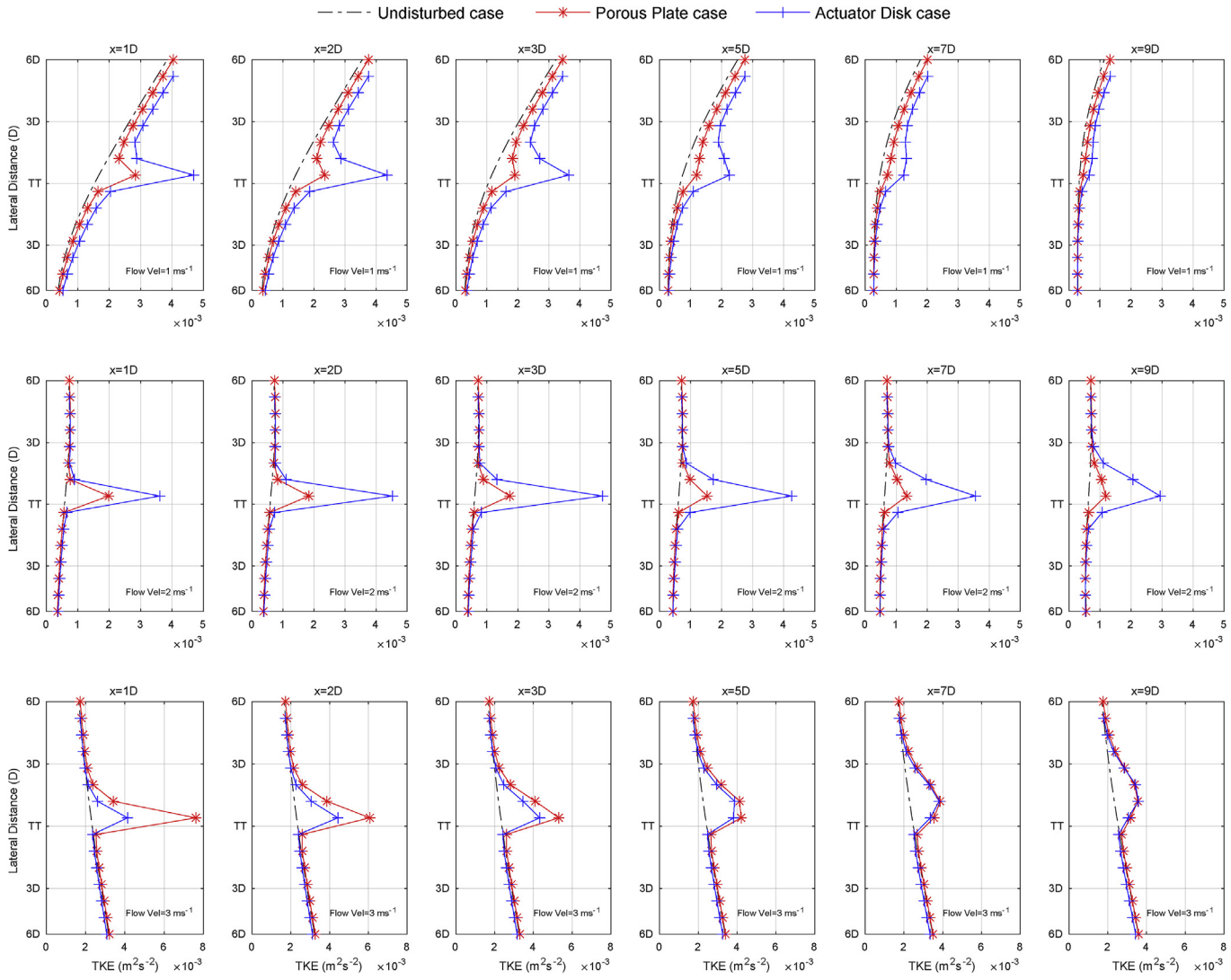

Fig. 13. Comparison between the Porous Plate and Actuator Disc approaches: Downstream impacts on the lateral profiles of the TKE at the HATT's hub water depth.

enhanced bottom friction or momentum losses stand out. Although those methodologies (e.g. *Porous Plate* tool in Delft3D-FLOW) present significant limitations (misrepresentations in turbine geometry and energy extraction), they are widely used in research dealing with far-field hydrodynamic impacts. Recently, Delft3D-FLOW has developed a new methodology (*Actuator Disc*) based on Momentum Actuator Disc Theory, which has shown excellent results against laboratory test data, overcoming most of the limitations of traditional methodologies. Therefore, the objective of this paper is to evaluate and compare the performance of the *Porous Plate* and *Actuator Disc* methodologies in terms of key hydrodynamic variables such as free surface elevation, instantaneous and residual flow velocity, and turbulence conditions.

Overall, the results obtained show that the traditional momentum sink approach (*Porous Plate*) struggles significantly to correctly reproduce the near and far wake patterns of instantaneous and residual flow velocity and turbulence conditions. The assumption of a constant loss coefficient for the *Porous Plate* approach, appears as the main limiting factor for correct estimation of the far-field hydrodynamics. On these grounds, the use of the *Porous Plate* plate approach may lead to considerable misrepresentation in terms of tidal resource assessment, tidal farm layout optimisation, transport of suspended matter and hydrodynamic loads on tidal turbines. Consequently, previous research, using Delft3D-FLOW together with the *Porous Plate* tool, to assess the impacts of tidal energy extraction on the flow conditions should be considered only as a first approximation.

In summary, this work explores the main benefits of applying Momentum Actuator Disc Theory within Delft3D-FLOW to assess the disruptions caused by tidal turbines on the far-filed

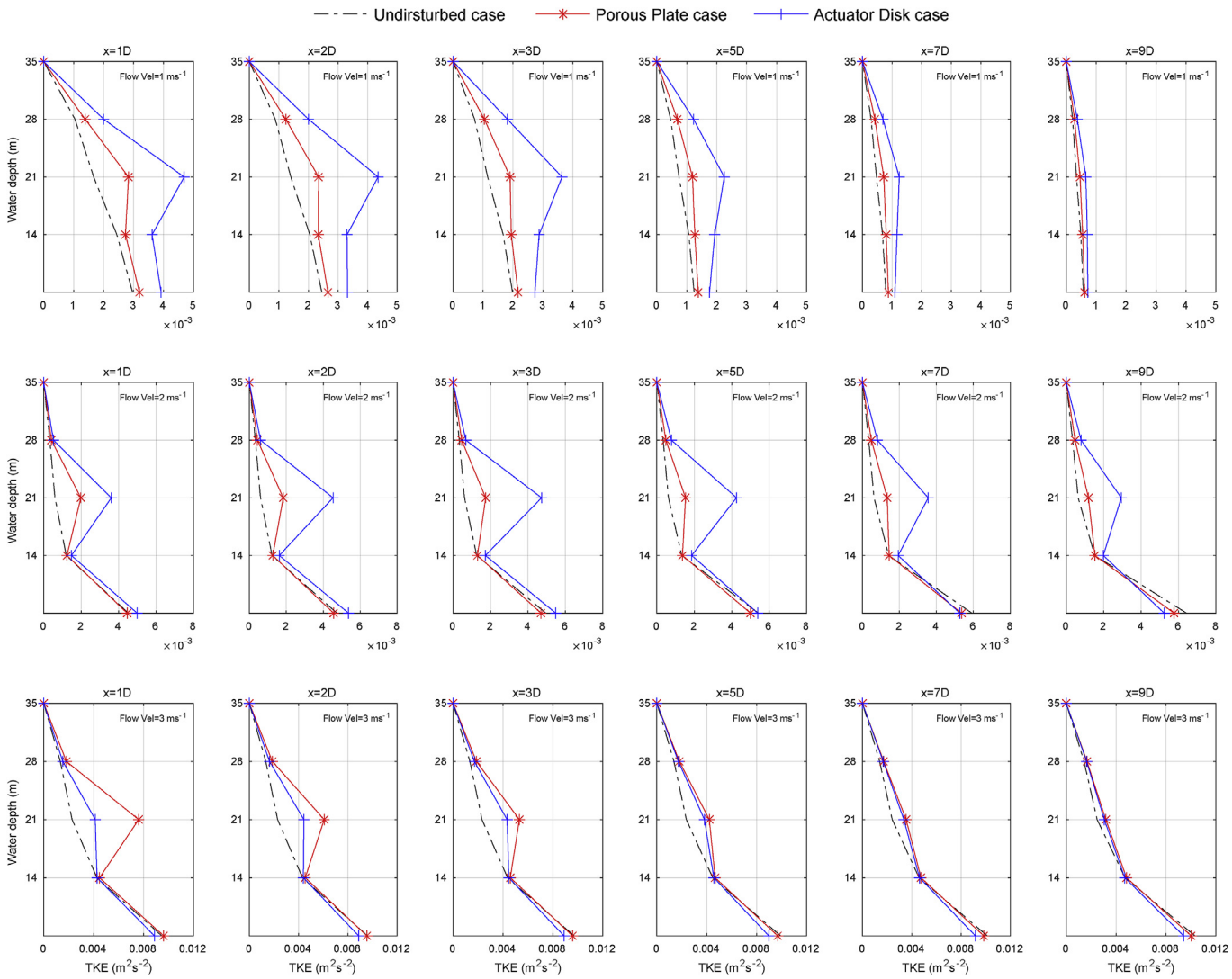

Fig. 14. Comparison between the Porous Plate and Actuator Disc approaches: Downstream impacts on the vertical profiles of the TKE.

hydrodynamics. In spite of the promising results obtained, further development to account for the turbulence induced by turbine operation is required, which will be dealt with in future lines of research.

Acknowledgments

During this work, V. Ramos was supported by the I2C post-doctoral grant ED481B 2014/059-0 (Plan Galego de Investigacion Innovacion e Crecemento 2011–2015) of the Xunta de Galicia (Spain). The authors are also indebted to the European Marine Energy Centre (EMEC) for its contribution with the ADCP data and the Irish Centre for High-End Computing (ICHEC) for its cooperation in the computational tasks.

References

[1] N. Johnstone, I. Haščič, D. Popp, Renewable energy policies and technological innovation: evidence based on patent counts, Environ. Resour. Econ. 45 (1) (2010) 133–155.
[2] E. Brito, A. Melo, J. Huckerby, Annual Report 2012. Implementing Agreement on Ocean Energy Systems, Tech. rep., IEA-OES, Lisboa, 2012.
[3] A.S. Bahaj, Generating electricity from the oceans, Renew. Sustain. Energy Rev. 15 (7) (2011) 3399–3416.
[4] R. Carballo, G. Iglesias, A. Castro, Numerical model evaluation of tidal stream energy resources in the Ria de Muros (NW Spain), Renew. Energy 34 (6) (2009) 1517–1524.
[5] Fergal O. Rourke, Fergal Boyle, Anthony Reynolds, Tidal energy update 2009, Appl. Energy 87 (2) (2010) 398–409.
[6] IEC-TS 62600-201, Marine Energy Wave, Tidal and Other Water Current Converters Part 201: Tidal Energy Resource Assessment and Characterisation, 2014.
[7] C. Zarzuelo, A. López-Ruiz, M. Díez-Minguito, M. Ortega-Sánchez, Tidal and subtidal hydrodynamics and energetics in a constricted estuary, Estuar. Coast. Shelf Sci. 185 (2017) 55–68.
[8] R. Malki, I. Masters, A.J. Williams, T.N. Croft, Planning tidal stream turbine array layouts using a coupled blade element momentum–computational fluid dynamics model, Renew. Energy 63 (2014) 46–54.
[9] S. Tedds, I. Owen, R. Poole, Near-wake characteristics of a model horizontal axis tidal stream turbine, Renew. Energy 63 (2014) 222–235.
[10] A. Bahaj, L. Myers, M. Thomson, N. Jorge, Characterising the wake of horizontal axis marine current turbines, in: Proceedings of the 7th European Wave and Tidal Energy Conference, University of Southampton Porto, Portugal, 2007, p. 9.
[11] P. Ouro, M. Harrold, T. Stoesser, P. Bromley, Hydrodynamic loadings on a horizontal axis tidal turbine prototype, J. Fluid Struct. 71 (2017) 78–95.
[12] S. Mungar, Hydrodynamics of Horizontal-axis Tidal Current Turbines: A Modelling Approach Based on Delft3D, 2014. https://repository.tudelft.nl.
[13] I. Milne, A. Day, R. Sharma, R. Flay, Blade loading on tidal turbines for uniform unsteady flow, Renew. Energy 77 (2015) 338–350.
[14] R. Vennell, S.W. Funke, S. Draper, C. Stevens, T. Divett, Designing large arrays of tidal turbines: a synthesis and review, Renew. Sustain. Energy Rev. 41 (2015) 454–472.

[15] V. Ramos, R. Carballo, M. Alvarez, M. Sanchez, G. Iglesias, Assessment of the impacts of tidal stream energy through high-resolution numerical modeling, Energy 61 (2013) 541–554.
[16] S.W. Funke, P.E. Farrell, M. Piggott, Tidal turbine array optimisation using the adjoint approach, Renew. Energy 63 (2014) 658–673.
[17] V. Ramos, R. Carballo, M. Sanchez, M. Veigas, G. Iglesias, Tidal stream energy impacts on estuarine circulation, Energy Convers. Manag. 80 (0) (2014) 137–149.
[18] S.P. Neill, J.R. Jordan, S.J. Couch, Impact of tidal energy converter (TEC) arrays on the dynamics of headland sand banks, Renew. Energy 37 (1) (2012) 387–397.
[19] M. Palm, R. Huijsmans, M. Pourquie, A. Sijtstra, Simple wake models for tidal turbines in farm arrangement, in: ASME 2010 29th International Conference on Ocean, Offshore and Arctic Engineering, American Society of Mechanical Engineers, 2010, pp. 577–587.
[20] G. Shapiro, Effect of tidal stream power generation on the region-wide circulation in a shallow sea, Ocean Sci. 7 (1) (2011) 165.
[21] S.C. Kramer, M.D. Piggott, A correction to the enhanced bottom drag parameterisation of tidal turbines, Renew. Energy 92 (2016) 385–396.
[22] S. Baston, S. Waldman, J. Side, Modelling Energy Extraction in Tidal Flows, MASTS, 2015, pp. 75–107, rev 3.1, TeraWatt Position Papers, http://www.masts.ac.uk/media/166596/position_papers_terawatt_e-book.pdf.
[23] Hydraulics, Delft, Delft, the Netherlands., Delft3D-FLOW User Manual, 2006.
[24] M. Sanchez, R. Carballo, V. Ramos, G. Iglesias, Floating vs. bottom-fixed turbines for tidal stream energy: a comparative impact assessment, Energy 72 (2014) 691–701.
[25] Delft3D Repository, Deltares, 2016. https://svn.oss.deltares.nl.
[26] T. Roc, D.C. Conley, D. Greaves, Methodology for tidal turbine representation in ocean circulation model, Renew. Energy 51 (2013) 448–464.
[27] T. Roc, D. Greaves, K.M. Thyng, D.C. Conley, Tidal turbine representation in an ocean circulation model: towards realistic applications, Ocean Eng. 78 (2014) 95–111.
[28] G.S. Stelling, On the construction of computational methods for shallow water flow problems, Rijkswaterstaat Commun. (1984) 226.
[29] I. UNESCO, Tenth report of the joint panel on oceanographic tables and standards, UNESCO Tech. Pap. Mar. Sci. 36 (1981) 15–19.
[30] W. Rodi, Turbulence Models and Their Application in Hydraulics, Routledge, 2017.
[31] S. Waldman, S. Baston, R. Nemalidinne, A. Chatzirodou, V. Venugopal, J. Side, Implementation of tidal turbines in MIKE 3 and Delft3D models of Pentland Firth & Orkney waters, Ocean Coast Manag. 147 (2017) 21–36.
[32] T. Stallard, R. Collings, T. Feng, J. Whelan, Interactions between tidal turbine wakes: experimental study of a group of three-bladed rotors, Phil. Trans. R. Soc. A 371 (1985), 20120159, 2013.
[33] M.C. Easton, D.K. Woolf, P.A. Bowyer, The dynamics of an energetic tidal channel, the Pentland Firth, Scotland, Cont. Shelf Res. 48 (2012) 50–60.
[34] V. Ramos, J.V. Ringwood, Implementation and evaluation of the international electrotechnical commission specification for tidal stream energy resource assessment: a case study, Energy Convers. Manag. 127 (2016) 66–79.
[35] J.M. Dias, J. Lopes, Implementation and assessment of hydrodynamic, salt and heat transport models: the case of ria de aveiro lagoon (Portugal), Environ. Model. Softw. 21 (1) (2006) 1–15.
[36] S.W. Funke, S.C. Kramer, M.D. Piggott, Design optimisation and resource assessment for tidal-stream renewable energy farms using a new continuous turbine approach, Renew. Energy 99 (2016) 1046–1061.
[37] R. Carballo, G. Iglesias, A. Castro, Residual circulation in the Ria de Muros (NW Spain): a 3D numerical model study, J. Mar. Syst. 75 (1–2) (2009) 116–130.
[38] M. Togneri, M. Lewis, S. Neill, I. Masters, Comparison of ADCP observations and 3D model simulations of turbulence at a tidal energy site, Renew. Energy 114 (2017) 273–282.
[39] T. Blackmore, L.E. Myers, A.S. Bahaj, Effects of turbulence on tidal turbines: implications to performance, blade loads, and condition monitoring, Int. J. Mar. Energy 14 (2016) 1–26.
[40] F. Maganga, G. Germain, J. King, G. Pinon, E. Rivoalen, Experimental characterisation of flow effects on marine current turbine behaviour and on its wake properties, IET Renew. Power Gener. 4 (6) (2010) 498–509.
[41] T. Nishino, R.H. Willden, Effects of 3D channel blockage and turbulent wake mixing on the limit of power extraction by tidal turbines, Int. J. Heat Fluid Flow 37 (2012) 123–135.
[42] Simon P. Neill, M. Reza Hashemi, Matt J. Lewis, The role of tidal asymmetry in characterizing the tidal energy resource of Orkney, Renew. Energy 68 (2014) 337–350.
[43] G. Iglesias, R. Carballo, Seasonality of the circulation in the ría de muros (nw Spain), J. Mar. Syst. 78 (1) (2009) 94–108.